SINCLAIR, R., GORINGE, M. J. & THOMAS, G. (1975). *Philos. Mag.* B32, 501-512.
TAKAMA, T. & SATO, S. (1982). *Philos. Mag.* B45, 615-625.
TERASAKI, O., WATANABE, D. & GJØNNES, J. (1977). *Proceedings of the Fifth International Conference on High-Voltage Electron Microscopy*, edited by T. IMURA & H. HASHIMOTO, pp. 263-266. Kyoto: Japanese Society of Electron Microscopy.
TERASAKI, O., WATANABE, D. & GJØNNES, J. (1979). *Acta Cryst.* A35, 895-900.
WATANABE, D., ANDERSSON, B. & GJØNNES, J. (1974). *Acta Cryst.* A30, 772-776.
WATANABE, D., UYEDA, R. & FUKUHARA, A. (1969). *Acta Cryst.* A25, 138-140.

Acta Cryst. (1984). B40, 549-554

High-Resolution Electron Microscopy Study of Polycrystalline Evaporated Titanium Monoxide Films

BY SHEN GUANG JUN AND L. A. BURSILL

School of Physics, University of Melbourne, Parkville, 3052 *Victoria, Australia*

K. YOSHIDA AND Y. YAMADA

College of General Education, Tohoku University, Kawauchi, Sendai 980, *Japan*

AND H. OTA

1*MV Electron Microscope Laboratory, Tohoku University, Katahira, Sendai* 980, *Japan*

(*Received* 6 *December* 1983; *accepted* 11 *June* 1984)

Abstract

High-resolution electron microscope (HREM) images of the δ phase of TiO_x ($0{\cdot}7 \le x \le 1{\cdot}0$) were analysed by comparison with computer-simulated images. This allowed a hexagonal structural model, proposed previously on the basis of powder X-ray data, to be confirmed using effectively single-crystal data for two projections of the structure. A study of the sensitivity of HREM images to crystal thickness and local variations in stoichiometry allowed (i) local variations in grain thickness to be assigned in the range 173 to 245 Å and (ii) the local stoichiometry to be assigned as $x = 0{\cdot}8$. The techniques developed should extend readily to studies of other polycrystalline thin films.

1. Introduction

The crystal structure of TiO_x ($0 \le x \le 1{\cdot}25$) varies with x, the Ti atom arrangement varying from essentially h.c.p. to essentially c.c.p. Thus the h.c.p. α phase occurs in the range $0 \le x \le 0{\cdot}5$, when oxygen atoms are included in tetrahedral interstices, and in the range $0{\cdot}5 \le x \le 0{\cdot}9$ a mixture of (α + TiO) phases may occur, depending upon thermal treatment (Roy & White, 1972). The Ti_2O phase represents one of the possible ordered arrangements of oxygen (Holmberg, 1962). The 'rock-salt' (c.c.p.) type TiO phase exists in the range $0{\cdot}7 \le x \le 1{\cdot}25$. This contains empty titanium and oxygen sites (Andersson, Collén, Kuglenstierna & Magnéli, 1957), which may become ordered following appropriate thermal treatments below 1260 K (Watanabe, Terasaki, Jostons & Castles, 1970). The so-called transition structure contains vacant sites of oxygen (Watanabe, Castles, Jostons & Malin, 1966) and titanium (Hilty, 1968) concentrated on every third (220) plane of the 'rock-salt' type structure. Such an ordering of space distorts the parent lattice (Hilty, 1968; Yamada 1983). The so-called δ phase may occur for $0{\cdot}53 \le x \le 0{\cdot}89$. Bumps, Kessler & Hansen (1953) reported its structure to be tetragonal, and this was apparently confirmed by Schofield & Bacon (1955-56). However, Andersson (1959) proposed a hexagonal structure for the δ phase. This was based upon an analysis of X-ray powder data. Since this phase apparently always coexists with α + TiO phases the structure analysis by single-crystal techniques was not possible. Yamada & Yoshida (1983) studied the phase transformation of evaporated films of $TiO_{0{\cdot}5}$ (α phase) into the TiO phase by *in situ* oxidation of evaporated thin films using an electron microscope, when a characteristic sequence of changes could be induced. Grains of the δ-phase precipitate during this transformation and Andersson's hexagonal unit-cell parameters for the δ phase were verified by analysing diffraction patterns taken from these single-crystal grains. The lattice parameters measured were nearly equal to those of Andersson, *i.e.* $A_\delta = 4{\cdot}99$ and $C_\delta = 2{\cdot}88$ Å.

In the present paper HREM images of the δ phase are presented for two projections of the structure.

0108-7681/84/060549-06$1.50

Image-matching techniques, using computer simulations, confirm the hexagonal structural model of Andersson. In addition, it is shown how these techniques can provide valuable information concerning the stoichiometry, thickness and topology of individual grains.

2. Experimental

A bulk crystal of $TiO_{1\cdot0}$ was evaporated onto a NaCl substrate held at 800 K. After being detached from the substrate the 300 Å thick film was heated at 850 K in a vacuum of 3–7 mPa in the specimen chamber of a JEM-7 electron microscope (Yamada, 1983). Changes in diffraction contrast images and in diffraction patterns were observed *in situ* during heating and the composition of the film was measured by an Auger electron spectrometer (Yamada & Yoshida, 1983).

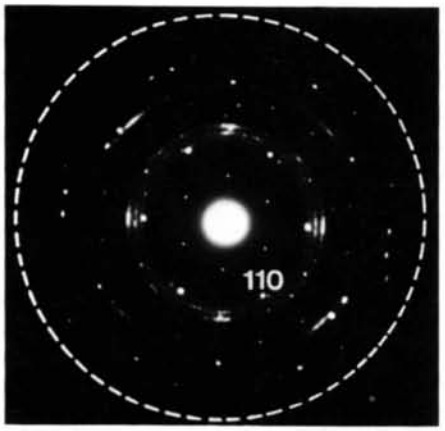

(*a*)

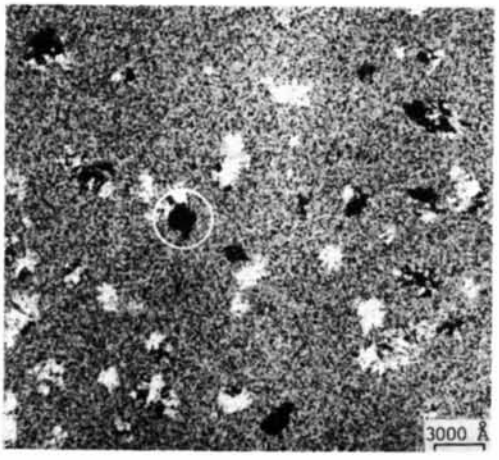

(*b*)

Fig. 1. (*a*) Diffraction pattern showing polycrystalline nature of TiO_x ($0{\cdot}7 \le x \le 0{\cdot}9$) thin film, after annealing at 850 K for *ca* 6 min. The diameter of the objective aperture used for high-resolution studies is indicated. (*b*) The corresponding diffraction contrast image shows many small crystallites. A relatively large crystallite (circled), giving rise to the hexagonal spot pattern shown within (*a*), was selected for HREM study.

The as-deposited film was composed of both the (α + TiO) phases, with the composition $TiO_{0\cdot5}$. After annealing at 850 K for 5 min the composition was *ca* $TiO_{0\cdot6}$ and crystallites of an ordered transition structure appeared. On annealing at 850 K for one further minute fine diffraction spots appeared suddenly (indicated in Fig. 1*a*) and precipitation of new crystallites occurred (Fig. 1*b*). It was verified readily, from selected-area diffraction patterns, that these were crystallites of the δ phase. The crystallites of the δ phase are larger than those of the α or TiO phase and may be up to several thousand ångströms in diameter. The composition of the film, including α + TiO + δ phases, now ranged from $TiO_{0\cdot7}$ to $TiO_{1\cdot0}$. High-resolution electron micrographs were taken with a JEM-1000 electron microscope with objective-lens pole pieces having spherical aberration coefficient $C_s = 11$ mm. The size of the objective aperture used for HREM is indicated in Fig. 1(*a*).

3. HREM observations

Fig. 2 gives a wide-field view of the area chosen for HREM. Many grains, having a variety of misorientations and sizes, may be seen. Small-angle grain boundaries are indicated by relatively broad fringes across which changes in image detail occur. Characteristic contrasts (labelled *A*, *B*, *C* and *D*) occur throughout the field. In this case $[00.1]_\delta$ is approximately parallel to the electron beam throughout most of the area. Even within this area, which shows essentially one grain and its immediate surroundings (~300 Å diameter), there are a wide range of local contrasts; labelled *A*, *B*, *C*, *D* and *E*, for example. [Further

Fig. 2. Relatively wide-field HREM image of the area circled in Fig. 1(*b*), showing lattice geometry which corresponds essentially to $[00.1]_\delta$ orientation throughout most of field. Broader fringes indicate low-angle grain boundaries inclined to foil normal. Characteristic contrasts (labelled *A*, *B*, *C*, *D* and *E*) show essentially hexagonal symmetries.

enlargements of these images are given below, Figs. 6(*a*)–6(*d*), when they are compared with computer simulations.] In all cases the arrangement of blobs is essentially hexagonal, revealing the unit-cell spacings 4·99 and 2·88 Å characteristic of the $[00.1]_\delta$ projection of the δ phase. The featureless area to the right in Fig. 2 probably consists of very fine-grain α- and/or TiO-phase material, indicated by diffuse spots and rings in the selected-area diffraction pattern (*cf.* Fig. 1*a*).

Fig. 3(*a*) gives a selected-area diffraction pattern from an area of the film containing a relatively large grain indicating the $[01.0]_\delta$ projection of the δ phase. Diffuse spots and rings again indicate coexistence with α + TiO phases. Fig. 3(*b*) shows a part of the HREM image from this grain, when the 4·32 and 2·88 Å lattice spacings appear. The image contrast is relatively uniform throughout, compared with Fig. 2.

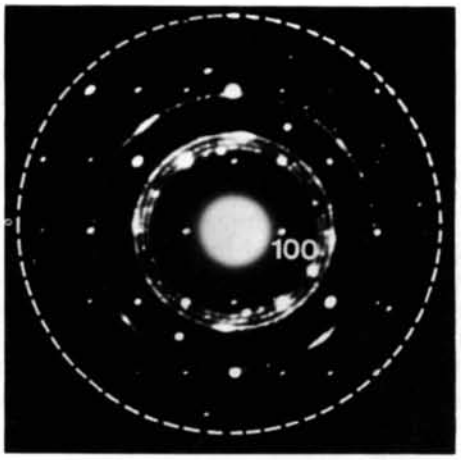

(*a*)

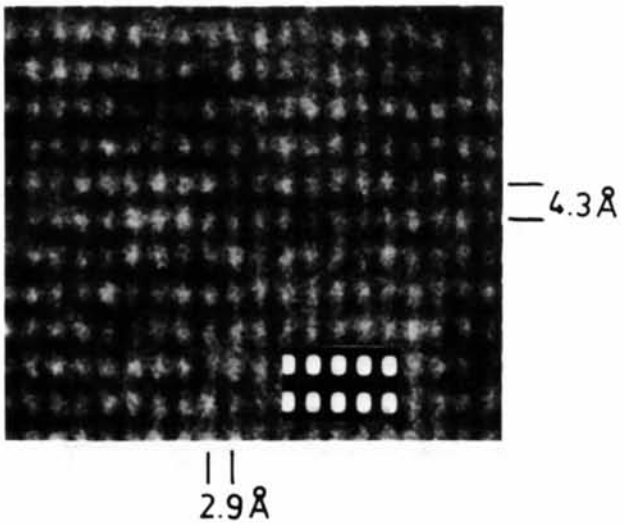

(*b*)

Fig. 3. (*a*) Selected-area diffraction pattern from a relatively large grain (*cf.* Fig. 5) showing $[01.0]_\delta$ rectangular pattern coexisting with diffuse spots and rings corresponding to α + TiO phases. (*b*) HREM image of grain showing $[01.0]_\delta$ lattice spacings. Image detail is relatively very uniform compared with Fig. 2. Note 4·32 and 2·88 Å lattice spacings. Inset shows computed image for $x = 0{\cdot}8$.

4. Computer simulation of HREM images

(*a*) *Structural model for δ-phase* TiO_x $(0{\cdot}7 \le x \le 1{\cdot}0)$

The atomic coordinates for computer simulations were taken from Andersson (1959), since both the earlier single-crystal electron diffraction analysis (Yamada & Yoshida, 1983) and the present HREM results are clearly consistent with the hexagonal cell parameters but do not correspond to the tetragonal cell reported by Bumps *et al.* (1953). Thus the space group was taken as *P6/mmm* (No. 191) with 1 Ti in 1(*a*) at 000; 2 Ti in 2(*d*) at $\frac{1}{3}\,\frac{2}{3}\,\frac{1}{2}$, $\frac{2}{3}\,\frac{1}{3}\,\frac{1}{2}$; and 3 O in 3(*f*) at $\frac{1}{2}\,0\,0$, $0\,\frac{1}{2}\,0$, $\frac{1}{2}\,\frac{1}{2}\,0$.

The structure is illustrated in Figs. 4(*a*) and 4(*b*), projected along $[00.1]_\delta$ and $[01.0]_\delta$, respectively. Large and small circles represent titanium and oxygen atoms, respectively. Open circles have $z = 0$ and filled ones $z = \frac{1}{2}$ in Fig. 4(*a*). The oxygen positions have mean occupancy x, presumably with a homogeneous distribution. The structure is described in detail by Andersson (1959) and its structural relationships with α-Ti_2O and Ti–O have been treated by Andersson (1960) and, from a different viewpoint, by Yamada & Yoshida (1983). Note that the metal-atom structure is *neither* h.c.p. nor c.c.p. The oxygen atoms occupy $[OTi_6]$ octahedrally-coordinated sites within the metal-atom array.

(*b*) *Image-simulation techniques*

Calculations were based upon the multislice formulation of the *N*-beam dynamical theory of electron scattering by crystals (Goodman & Moodie, 1974) using recent modifications of the computer programs (Wilson, 1981). The electron energy was taken as 1 MV with spherical aberration coefficients C_s = 11 mm, as appropriate for the JEM-1000 instrument in Sendai. Preliminary calculations indicated that the effective instrumental resolution was approximately 2·4 Å for the present images.*

Figs. 5(*a*), 5(*b*) show the variation with increasing thickness of the amplitudes and phases of low-order beams for the $[00.1]_\delta$ projection of $TiO_{1\cdot0}$. The maximum grain thickness is ~300 Å, the same as that of the as-deposited film (Yamada & Yoshida, 1983). Note the quasi-periodicity of approximately 100 Å for the transmitted beam 000, which reflects the oscillations in 110 and 300 of *ca* 80 and 140 Å, respectively. Note the discontinuity in the variation of phase

* More recent images, for other materials, indicate 1·8 Å resolution may now be achieved (Hiraga, Tsuno, Shindo, Hirabayashi, Hayashi & Hirai, 1983).

for the 110 beams of thickness $H = 100$ Å and the oscillations in phase of both 110 and 300 beams. Since 110 beams are directly effective in forming the image (Fig. 5*a*) a strong thickness dependence of image contrast may be anticipated. It is clear from Fig. 2 that the grain thickness is changing rapidly, at least around its periphery. Images were therefore calculated for a range of thickness $0 \leq H \leq 350$ Å. Fig. 2 was actually the fourth of a through-focal series of images recorded from the same area, at defocus intervals (Δf) of 500 Å. Owing to the continuous nature of the film the initial defocus condition could not be controlled precisely, for example by studying the behaviour of the Fresnel fringe or contamination of the film. However, assuming $\Delta f = 0$ for the first image we deduce $\Delta f = -1500$ Å for Fig. 2. In fact, through-focal series of images were calculated initially for $-1800 \leq \Delta f \leq +200$ Å, although comparisons with the experimental images established that the defocus range $-1800 \leq \Delta f \leq -1500$ Å was most appropriate for image matching. In order to allow for possible effects of variations in local stoichiometry on the image contrast it was necessary to repeat the simulations for $x = 0{\cdot}7$, $0{\cdot}8$, $0{\cdot}9$ and $1{\cdot}0$. The effect of x on the variation of amplitude and phase of the transmitted beam showed that the images will be sensitive to x for $200 \leq H \leq 350$ Å. In effect the computer simulations lead to a large matrix of images, showing variations with crystal thickness, stoichiometry (resolution, initially) and objective-lens defocus.

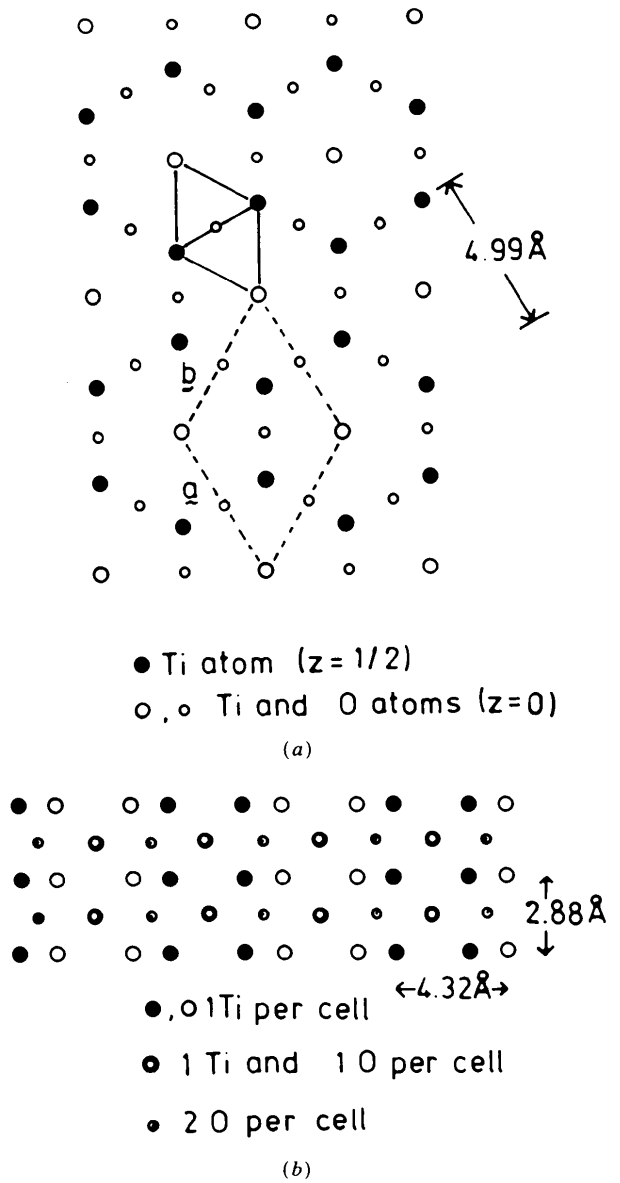

Fig. 4. The crystal structure of δ-TiO_x, projected along (*a*) $[00.1]_\delta$ and (*b*) $[01.0]_\delta$. Large and small circles represent titanium and oxygen atoms, respectively. Open circles have $z = 0$ and filled ones $z = \frac{1}{2}$ (in *a*). The oxygen positions are partially unfilled, presumably with a homogeneous distribution.

(*c*) *Image-matching procedure*

The characteristic contrasts labelled *A*, *B*, *C* and *D* (Fig. 2) were selected for image matching. Since the film was only 300 Å thick and the image contrast was not strongly dependent upon objective-lens defocus steps of ≤ 100 Å or on stoichiometry changes $\Delta x = 0{\cdot}1$, it was assumed initially that $\Delta f = -1500$ Å and that the predominant factor in changing contrast

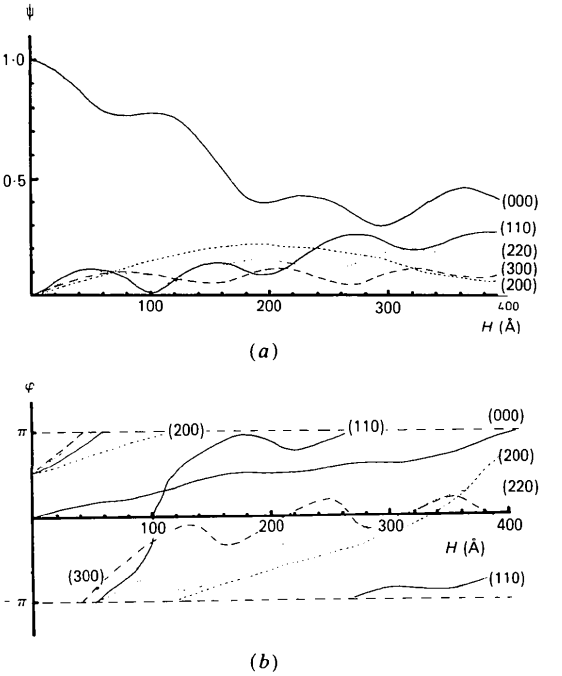

Fig. 5. Variation with thickness of (*a*) amplitudes and (*b*) phases of low-order reflections for the $[00.1]_\delta$ projection of $TiO_{1\cdot0}$. Note the smooth variation for most reflections, but oscillations (quasi-period ~80 and 120 Å) for 110 and 300 beams. Note also discontinuity in phase for 110 at $H = 100$ Å.

Table 1. *Location of characteristic images A, B, C and D (Fig. 3) with respect to crystal thickness H(Å) and objective-lens defocus Δf(Å)*

$\tilde{A}$ means that the image is similar to *A*.

$-\Delta f$	−1300				−1600				−1700			
H	0·7	0·8	0·9	1·0	0·7	0·8	0·9	1·0	0·7	0·8	0·9	1·0
143·9											*B*	*B*
158·3					*B*						*B*	*B*
172·7			$\tilde{A}$	$\tilde{A}$		$\tilde{A}$		*B*	*B*	*B*	*B*	
187·1			$\tilde{A}$	$\tilde{A}$		$\tilde{A}$					*B*	
201·5	*A*	*A*			*A*			*D*	*A*	$\tilde{A}$		
213·9											*D*	*D*
230·3								*D*		*D*	*D*	
244·7								*D*		*C*	*C*	
259·1												
273·3						*D*						
287·9							*D*					
302·3						*D*	*D*					
316·7			*D*	*D*			*D*			*D*	*D*	*C*
331·1							*C*			*D*		
343·3							*C*					
359·9												*B*
374·3												
388·7												
403·1												

was local variation of crystal thickness across the grain. The effect of Δf and then stoichiometry were investigated at a later stage. Thus, the simulated images were classified as *A*, *B*, *C* or *D* type and a table was constructed (see Table 1) indicating the variation with crystal thickness, defocus and stoichiometry. Clearly, any one of the characteristic images *A*–*D* may be found for quite diverse values of the experimental parameters. There does not appear to be a direct analytical route to a unique solution for the image match. It was possible, nevertheless, to find a combination of crystal-thickness variations (indicated in Table 1) for $\Delta f = -1700$ Å and $x = 0{\cdot}80$ which gave a reasonably smooth variation of contrast for $173 \leq H \leq 245$ Å, which was consistent with the experimental result of Fig. 2. Detailed comparisons of computed and observed characteristic images are shown in Fig. 6(*a*)–(*d*). In fact, the requirement of having a smooth sequence in thickness variation (*without* sharp changes in Δf and x) across the field of Fig. 2 provided a severe constraint in assigning Δf and x. Thus, whilst it is not reasonable to claim that the assigned values of H, Δf, and x provide a unique image match it is necessary to note that we were unable to find an alternative set which gave even remotely as convincing an image match.

The variation with thickness of the amplitudes and phases of the 000, 001, 100 and 101 beams for the $[01.0]_\delta$ projection were far less sensitive to thickness than was the case for the $[00.1]_\delta$ projection. Thus, image matches for the $[01.0]_\delta$ projection could be obtained for a wide range of thickness, Δ_f and x, values [an example is inset in Fig. 3(*b*) for $x = 0{\cdot}8$]. Clearly, images for this zone are not useful for precise determination of crystal thickness or stoichiometry.

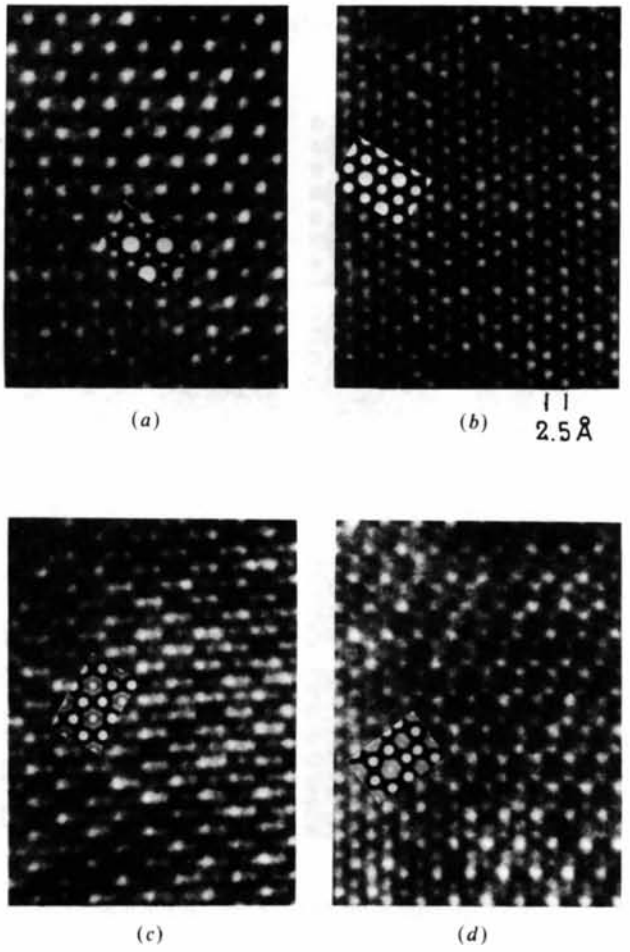

Fig. 6. Best-fit image matches obtained for characteristic images *A*, *B*, *C* and *D*, providing a smooth variation in thickness *H* across the field of Fig. 2. ($\Delta f = -1700$ Å, $x = 0{\cdot}8$, *cf.* Table 1.)

5. Discussion

It appears from Table 1 and Fig. 6 that the structural model of Andersson must be essentially correct. Thus, a series of images, which are very sensitive to crystal thickness, objective-lens defocus and stoichiometry x, may be image matched. The range of crystal thicknesses involved, $173 \leq H \leq 245$ Å, is very reasonable given the observed topology (Fig. 2) of the polycrystalline film and its independently measured thickness of 300 Å. The HREM images thus provide valuable 'single-crystal' and topological data, which complement the previously analysed X-ray powder data in this case. So far we have not found evidence for short-range ordering within δ-phase TiO_x ($0{\cdot}7 \leq H \leq 1{\cdot}0$).

It should be noted that it was necessary to avoid selecting areas for image matching which were misoriented with respect to the incident beam. Thus, low-symmetry lattice images were excluded as being uncharacteristic. Similarly, areas where there was obviously more than one grain overlapping along the projection axis were excluded. These could only be image matched successfully if the orientation of both grains was known precisely. It was not considered worthwhile to attempt to deduce orientation relationships for such areas from the micrographs.

Further calculations showed that $[00.1]_\delta$ projection images become sensitive to stoichiometry (x) for thicker specimens ($H \geq 200$ Å). Thus, Figs. 7(a)-7(d) show images for $x = 0{\cdot}7$, $0{\cdot}8$, $0{\cdot}9$ and $1{\cdot}0$ computed for the Scherzer defocus condition ($\Delta f = -1130$ Å) and resolution 1·8 Å. Four crystal thicknesses were chosen for simulation, namely $H = 40$, 296, 360 and 400 Å. For $H = 40$ Å (thin-crystal 'structure-image' condition) there is virtually no visible variation with x. However, for $H = 296$, 360 and 400 Å the images (Figs. 7b-7d) do become readily distinguishable for $0{\cdot}7 \leq x \leq 0{\cdot}9$, with only small differences for $0{\cdot}9 \leq x \leq 1{\cdot}0$. It is suggested therefore that if, in future work, the crystal thickness may be independently assigned, then it should be possible to study local variations in stoichiometry (for $0{\cdot}7 \leq x \leq 0{\cdot}9$). It should also be possible to determine the topology of the thin film, and possibly also film thickness, using scanning electron microscopy (SEM) or scanning transmission (STEM) techniques, at the same time as HREM images are recorded.

Further attempts to study the structure of this and other TiO_x phases, using the combination of *in situ* annealing, HREM, SEM and Auger analysis, are continuing.

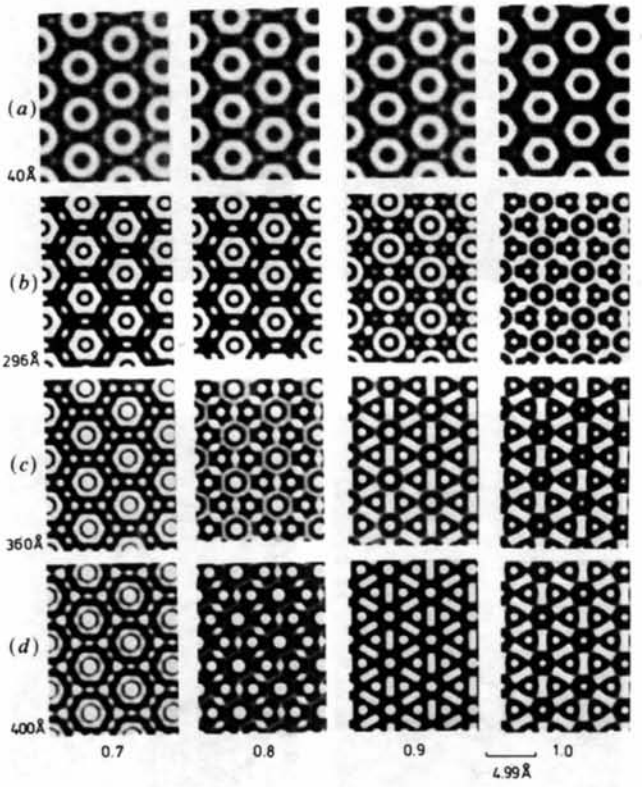

Fig. 7. Simulated images for TiO_x ($x = 0{\cdot}7$, $0{\cdot}8$, $0{\cdot}9$ and $1{\cdot}0$) for Scherzer defocus ($\Delta f = -1130$ Å) and (a) $H = 40$, (b) 296, (c) 360 and (d) 400 Å. Note thin-crystal 'structure images' are *not* sensitive to stoichiometry, whereas for thicker crystals $x = 0{\cdot}7$, $0{\cdot}8$ and $0{\cdot}9$ may be readily distinguished, although $x = 0{\cdot}9$ and $1{\cdot}0$ become far less distinguishable.

This work was financially supported by the Tohoku University and the University of Melbourne. K. Yoshida is grateful for the support of the Japanese Society for the Promotion of Science, for a visit to Melbourne during 1983, and Shen Guang Jun is grateful for the support of the Education Department of China.

References

ANDERSSON, S. (1959). *Acta Chem. Scand.* **13**, 415-419.
ANDERSSON, S. (1960). *Ark. Kemi*, **15**, 247-252.
ANDERSSON, S., COLLÉN, B., KUGLENSTIERNA, U. & MAGNÉLI, A. (1957). *Acta Chem. Scand.* **11**, 1641-1648.
BUMPS, E. S., KESSLER, H. D. & HANSEN, M. (1953). *Trans. Am. Soc. Met.* **45**, 1008-1028.
GOODMAN, P. & MOODIE, A. F. (1974). *Acta Cryst.* A**30**, 280-290.
HILTY, E. (1968). *Naturwissenschaften*, **55**, 130-131.
HIRAGA, K., TSUNO, K., SHINDO, D., HIRABAYASHI, M., HAYASHI, S. & HIRAI, T. (1983). *Philos. Mag.* A**47**, 483-496.
HOLMBERG, B. (1962). *Acta Chem. Scand.* **16**, 1245-1250.
ROY, R. & WHITE, W. B. (1972). *J. Cryst. Growth*, **13/14**, 78-83.
SCHOFIELD, T. H. & BACON, A. E. (1955-56). *J. Inst. Met.* **84**, 27-31.
WATANABE, D., CASTLES, J. R., JOSTONS, A. & MALIN, A. (1966). *Nature (London)*, **210**, 934-936.
WATANABE, D., TERASAKI, O., JOSTONS, A. & CASTLES, J. R. (1970). *The Chemistry of Extended Defects in Non-metallic Solids*, pp. 238-258. Amsterdam: North Holland.
WILSON, A. R. (1981). PhD Thesis, Univ. of Melbourne.
YAMADA, Y. (1983). *Jpn. J. Appl. Phys.* **22**, 29-35.
YAMADA, Y. & YOSHIDA, K. (1983) *Jpn. J. Appl. Phys.* **22**, 36-41.